Sustainable ammonia synthesis from seawater and nitrogen by single-step plasma catalysis: a step towards New England's farmers nitrogen autonomy

Hoang M. Nguyen[†], Fnu Gorky[†], Shelby Guthrie [†], Maria L. Carreon[*,†]

[†] Mechanical Engineering Department, University of Massachusetts Lowell, One University Avenue, Lowell, Massachusetts 01854-5043, USA.

Corresponding Author

E-mail address: Maria_Carreon@uml.edu (Maria L. Carreon).

ABSTRACT. Ammonia synthesis at ambient conditions employing intermittent green sources of energy and feedstocks is globally sought to replace the Haber-Bosch (H-B) process operating at high temperature and pressure. We report herein for the first time an effective and sustainable ammonia synthesis pathway from seawater and N_2 over a spherical SiO_2 and M/SiO_2 (M: Ag, Cu, and Co) catalysts driven by non-thermal plasma (NTP). Experimental results indicate that the presence of a catalyst is required for ammonia production from seawater and N_2. The Co/SiO_2 catalyst delivered the highest ammonia synthesis rate (r_{NH_3}) of 3.7 mmol.g_{cat}^{-1}.h^{-1} and energy yield of 3.2 $g_{NH_3}.kW^{-1}.h^{-1}$ at a relatively low input power of 2 W. The extraction of H atom from H_2O (seawater) molecules plays an important role in the ammonia synthesis from seawater. This work unfolds a novel platform for the subsequent optimization of sustainable ammonia production from endless resources such as seawater and N_2 through catalytic non-thermal plasma potentially powered by renewable sources.

KEYWORDS: Non-thermal plasma, plasma catalyst, sustainable ammonia synthesis, silica catalyst, seawater for ammonia.

INTRODUCTION

Ammonia plays a crucial role in the agricultural industry as a primary element for fertilizer production and it is also a foundational feedstock for pharmaceuticals, dyes, and chemical synthesis.[1] Ammonia has also emerged as an energy carrier and transportation fuel. Ammonia consists of 17.6 wt % of hydrogen, and thereby, it can be used as an indirect hydrogen storage compound.[2] Moreover, ammonia's energy density is approximately 4.32 $kWh.L^{-1}$, showing a capacity equivalently to methanol and almost double than that of liquid hydrogen.[3] Recently, automobiles operating on pure ammonia and gasoline-ammonia fuel modifications are being hypothesized and near to being prototyped.[4, 5] An important advantage of using pure ammonia is the resulting diminished reliance on fossil fuels by changing to a "sustainable fuel source" that can be manufactured synthetically.[6] In the near future synthetic low-carbon fuels will be needed as a response to the current environmental emergency, and ammonia is among such synthetic fuels.

Currently, the most commonly-used technology for ammonia production is the Haber-Bosch (H-B) process, which requires high energy input and emits greenhouse gas largely to achieve its harsh operating conditions i.e., high reaction temperature (400 – 500 ^{o}C) and high pressure (150 – 300 atm).[7-9] Such large intrinsic carbon footprint technology for ammonia synthesis secure a long-standing need for the development of alternative processes that operate under milder conditions such as low temperature, atmospheric pressure, and even more preferably, with zero carbon emissions. A possible solution to fulfill this goal is the use of regionalized synthesis processes powered by renewable energy resources, which can even exploit benefits from local resources, particularly in remote areas. Another challenge of the current ammonia synthesis is the use of "expensive" feed i.e., hydrogen. While hydrogen is considered a "green fuel" to replace fossil fuels, the use of such a valuable chemical as a feedstock for ammonia production is uneconomical. More importantly, the energy cost of hydrogen production originates from the energy-intensive methane reforming processes operated at 800-1000 ^{o}C.[10] The produced hydrogen also needs to be stored and transported,

posing safety concerns, and high downstream costs.[11] Therefore, alternative sustainable pathways for ammonia production will draw important attention from researchers and industries. The use of H_2O as a hydrogen source in the synthesis of ammonia is one of the most promising approaches when employing non-thermal plasma (NTP) in a sustainable and economical way. Nonetheless, most of the studies on the production of ammonia from N_2 and H_2O have been focused on photochemical, electrochemical routes, or hybrid plasma-activated electrolysis.[12-17] These processes are reported to operate under mild conditions. Despite the N_2 reduction determining the final ammonia synthesis yield there is an important competition with the hydrogen evolution reactions from such electrochemical-based processes, which are challenging to control.[18, 19] In addition, the electron energy transferred to N_2 molecules in these two processes is insufficient to dissociate its stable bonding energy (N≡N, 9.8 eV), and thereby, the resultant ammonia production rate is relatively low.[20, 21] Electrochemical processes for hydrogen production from water splitting is currently far from industrial application because of technical problems associated with electrode stability and electrolyser design/scale-up.[18] Hybrid plasma-electrochemical systems reducing N_2 with water show high potential for scale-up with high ammonia yield.[22] Nevertheless, such systems are complicated and require high capital investment to obtain a desirable high ammonia synthesis yield. In comparison to the mentioned processes, non-thermal plasma with highly energetic electrons, and in the presence of a catalyst i.e., plasma catalytic system can result in the activation of the highly stable N_2 molecules into more reactive, vibrationally or electronically excited states, enabling thermodynamically unfavourable reactions to occur at ambient conditions on selected catalytic surfaces.[23, 24] Moreover, dielectric barrier discharge (DBD) plasma reactors can be straightforward turned on/off suitable for storing intermittent energy.[25] This added to their conceptualization as modular small-scale systems for ammonia synthesis results in simple lightweight units compared to high pressure thermal reactors, which comprise added complex insulation/cooling systems.[26] Indeed, our group has studied ammonia synthesis over NTP

catalytic processes over the past years.[27-32] The achieved fundamental understanding on the effects of different catalysts, plasma-catalyst synergisms, and energy efficiency on ammonia synthesis allow us to primarily estimate the great potential of ammonia synthesis from N_2 and "green" H_2 sources, which is an important step to achieve zero-carbon ammonia synthesis. In fact, Zhou and co-workers are pioneers[33, 34] to substitute H_2 by water for plasma-assisted ammonia synthesis over a notable supported Ru catalyst and obtain an ammonia synthesis rate of around 2.7 $mmol.g_{cat}^{-1}.h^{-1}$. The potential implementation of non-thermal plasma technology will not be feasible until there is a competitive plasma catalytic system in terms of material selection and reactor design. New approaches are needed for intelligent design of catalyst materials and the chosen materials must pair well with efficient plasma reactors. As a choice of catalytic materials, solid oxides are robust and efficient low-cost materials for catalytic applications. Besides their low cost, they offer textural, compositional, and morphological properties that can be tailored for diverse targeted catalytic reactions.[35] Specially, silica is an appealing material for plasma catalytic ammonia synthesis due to: (i) SiO_2 lower electrical resistivity that can lead to more stable and uniform plasma discharges; [36] (ii) readiness to dissolve hydrogen;[37] (iii) weak bonding with nitrogen;[38] (iv) high thermal and chemical stability in the presence of water, which is the source of hydrogen in this work. Our catalyst selection is supported by our group's previous experience on rational design of catalysts for ammonia synthesis.[27, 30, 39] Moreover, it has been indicated that silica-based catalysts promote the decomposition of N_2O,[40, 41] which is an unwanted by-product during ammonia production from water and N_2.[33]

Given its wide availability, seawater is the most sustainable replacement for hydrogen in ammonia synthesis powered by NTP. The described challenges and opportunities have motivated us to substitute of H_2 by seawater during the synthesis of ammonia powered by a dielectric-barrier discharge (DBD) non-thermal plasma. To benchmark the ammonia synthesis rate from seawater and N_2, a feed mixture of H_2 and N_2 was also employed for NTP-assisted

ammonia synthesis. We have found an excellent ammonia synthesis rate of 3.7 mmol.g_{cat}^{-1}.h^{-1} and energy yield of 3.2 $g_{NH_3}.kW^{-1}.h^{-1}$, both better than previously obtained, at a low plasma input power of 2 W over the Co/SiO_2 catalyst. The results also primarily indicate the correlations between NO_x formation, catalysts, and ammonia synthesis rate. Mechanistic insights of ammonia formation pathways from N_2 and seawater are elucidated. This work demonstrates a straightforward single-step process to dissociate both seawater and N_2 molecules driven by atmospheric catalytic NTP without an extra energy-intensive conversion to produce ammonia sustainably and economically.

EXPERIMENTAL SECTION.

Chemicals and materials. Polyethylene-block-poly(ethylene glycol) (Sigma Aldrich, average Mn ~920), deionized water, tetraethyl orthosilicate (TEOS, Sigma Aldrich, 99.9%), toluene (Sigma Aldrich, 99.5%), silver nitrate (Sigma Aldrich, 99.5%), cobalt nitrate (Sigma Aldrich, 99.5%), copper nitrate (Sigma Aldrich, 99.5%), ammonium hydroxide solution (NH_4OH, 32 %, Sigma Aldrich), polystyrene microspheres (PS, Sigma Aldrich), and ethanol (70%, Sigma Aldrich). Seawater was collected from Rockport, Massachusetts, USA and used directly without further processing (**Figure S1**).

Catalyst preparation.

Synthesis of silica spheres. A first solution is formed by mixing 100 g of ethanol and 40 mL of NH_4OH and 6 g of Polyethylene-block-poly (ethylene glycol). A second solution consisting of 40 g toluene, 4 g PS beads, and 20 g deionized water is prepared. These two solutions were stirred separately for 30 mins before mixing together and stirring for 2 hrs. Then, 26 g of TEOS was added to the solution and kept stirring for 10 hours at 90 ^oC and 360 rpm. The obtained white gel was calcined at 650 ^oC for 4 h with a heating rate of 1 $^oC \cdot min^{-1}$ in air.

Synthesis of silica supported metal catalysts. The M/SiO_2 (M: Ag, Cu, and Co) catalysts were prepared by incipient wetness impregnation method using metallic nitrates as precursors. The samples were calcined at 500 °C for 4 hrs with a heating rate of 1 $^oC.min^{-1}$. The nominal

metal fraction was calculated by the ratio of metal mass (g) from its respective salt per the SiO_2 mass. This step aims to secure the metal content of 3 wt.% in the prepared catalysts to silica support.

Catalyst characterization. Powder X-ray diffraction (XRD) patterns were collected on a 3rd generation Empyrean, Malvern Panalytical (Cobalt Source), operated at 45 mA and 40 kV. The diffraction peaks were collected over a range of 2θ of 10-70° with a scanning step size of 0.01° and a time of 2 s. Raman Spectroscopy was employed for detailed molecular interaction and the disparity in morphology for the respective catalyst; the experiments were conducted under room temperature in a Micro-Raman Spectrometer and Raman microscope (Foster and Freeman) at 638 nm with accessible laser output power between 4.5-5 mW (maximum power output of 9 mW). All catalysts were tested at multiple points over microscopic slides in pentaplicates and further averaged. For the presented data, the instrument was calibrated before each sample was loaded, the catalyst was carefully spread on a polystyrene microscopic slide (25*75 mm). The average scanning time (15-18 seconds/scan) was automated via FORAMX3 software. Counts were increased to 10 for refining the Raman shifts (cm^{-1}). Raman bands are often influenced by strain, particle distribution, vibration bands of amorphous silica and presence of surface species. For presented data, the wavelength of 638 nm was selected for sharp visualization of peaks and lower signal-to-noise ratio at higher wavenumber (cm^{-1}). The morphologies of the catalysts were characterized by using scanning electron microscopy (SEM) JEOL JSM-7401F, with an acceleration voltage of 5 kV. The metallic concentration was verified by using ICP-OES equipment (NexION™ 350D-Optima 8300, PerkinElmer). Whereby, 1 mg of each catalyst sample was digested in a 5 % HNO_3 solution prior to analysis. The measurement was performed at room temperature and in triplicates.

Plasma-driven ammonia synthesis reaction. The experimental setup is shown in **Figure S2**. For the ammonia synthesis reaction from N_2/seawater reactants, different input N_2 flowrate were employed i.e., 3.1, 6.2, 12.5, and 25.0 sccm. Similar input N_2 flowrate range was

employed in ammonia production from N_2/H_2 mixtures with the input H_2 flowrate fixed at 12.5 sccm. Seawater was contained in a 500 mL DURAN© washing flask container. The relative humidity (RH%) of inlet N_2 gas was 100 % at 20 ºC and atmospheric pressure.[33] The effluent headline of the input N_2 gas pipeline was dipped to the bottom of the seawater container to secure maximum humidity with seawater. This step was performed at room temperature. The humid gas was passed through a packed-bed DBD reactor made of quartz tube (I.D. of 4 mm and O.D. of 6.40 mm) with coaxial tungsten rod electrode (2.4 mm diameter) and copper mesh grounding. The inner electrode is made of tungsten, and it is placed at the center of a quartz tube. For each experiment, 100 mg of catalyst in fine powder form was packed into the center of the quartz tube reactor. The quartz fritz was placed at the input and output of the reactor to prevent any possible catalyst displacement under the gas flow. To ensure that all ammonia is captured, the gas was bubbled in deionized water. The reactor exhaust is connected directly to an Agilent 8860A GC operating with a HP-PLOT U column (30 m × 0.32 mm × 10 μm) with hydrogen gas as a carrier. The light emitted from the discharge was led through an optical system. The measurements were recorded using a dual channel UV−vis−NIR spectrophotometer (Avantes Inc., USB2000 Series) in a scope mode. The spectral range was from 200 to 1100 nm, using a line grating of 600 lines/mm and a resolution of 0.4 nm. A bifurcated fibre optic cable of 400 μm was employed. Acceptance angle and location: emission spectra of the glow region were measured at the center of the tube since the catalyst was packed in the center of the tube. The fiber optical cable was positioned at the center of the reactor, and the distance between the reactor and fiber optical cable was 7 cm, consistent throughout the collection. The UV−vis−NIR spectrophotometer focuses the exit light under 90 °. Standard optical fibers have a numerical aperture of 0.22 and an acceptance angle of 25°.

RESULTS AND DISCUSSION

Catalytic characterization. Figure 1 presents the characterization results for the silica catalyst sample employed in this work. The scanning electron microscopy (SEM) image of the SiO_2

(**Figure 1(a)**) and the Co/SiO_2 (**Figure 1(b)**) indicates the presence of spherical particles surrounded by shapeless agglomerations. It is indicated that the spherical morphology is the most stable shape achieved in nature.[42] Being used as catalysts for chemical reactions, spherical structures provide high mechanical strength, short pathways for diffusion of species, dispersion enhancement due to the stabilization of electrostatic charges, and high surface area to volume ratio.[43,44,45] The presence of such spherical particles in the catalysts is expected to promote the ammonia synthesis yield. The impregnation of metals i.e., Co on the SiO_2 did not alter the morphology of the silica significantly (**Figure 1(b)**). The X-ray diffraction (XRD) reveals only a broad peak at 2θ of 26.08 ° (JCPDS 05–0492), implying the amorphous structure of the silica (**Figure 1(c)**). The SiO_2-related diffraction peak area was smaller in the impregnated catalysts. This is due to the competition with the sharp diffraction peaks of metals (Ag, Co, and Cu) in the approximate regions. Moreover, the diffraction peaks of Ag (JCPDS #04-0783), Co_3O_4 (JCPDS #42-1467), and CuO (JCPDS #80-1916) were well-detected from the Ag/SiO_2, Co/SiO_2, and Cu/SiO_2 catalysts, respectively. The ICP-OES of the Co/SiO_2, Ag/SiO_2, and Cu/SiO_2 catalysts verified the respective metallic content was 3.02, 3.10, and 3.04%, respectively. The Raman spectrum was collected from 1000 – 3500 cm^{-1} wavelengths for all catalyst samples (**Figure 1(d)**). The peak at 1000 to 1300 cm^{-1} are associated with Si while the peaks at 1500 – 1600 cm^{-1} are assigned to the photoluminescence of interstitial oxygen from atmospheric air in the interparticle space, respectively.[46-48] Such interstitial oxygen lead to the formation of a Frenkel defect pair (Si–Si bond and interstitial oxygen atom, O) by dense electronic excitation, and could have an effect on the catalytic activity of the prepared catalysts, which will be discussed below. There are unknown peaks appearing between 2500 and 3000 cm^{-1}. These bands appear with the laser excitation (λ_{exc}) at 514.5 nm possibly due to either linearly coordinated resonance phenomena[49] or the presence of small amounts of carbon, derived from organic surfactants employed during catalyst preparation, attributed to incomplete removal after calcination in air.

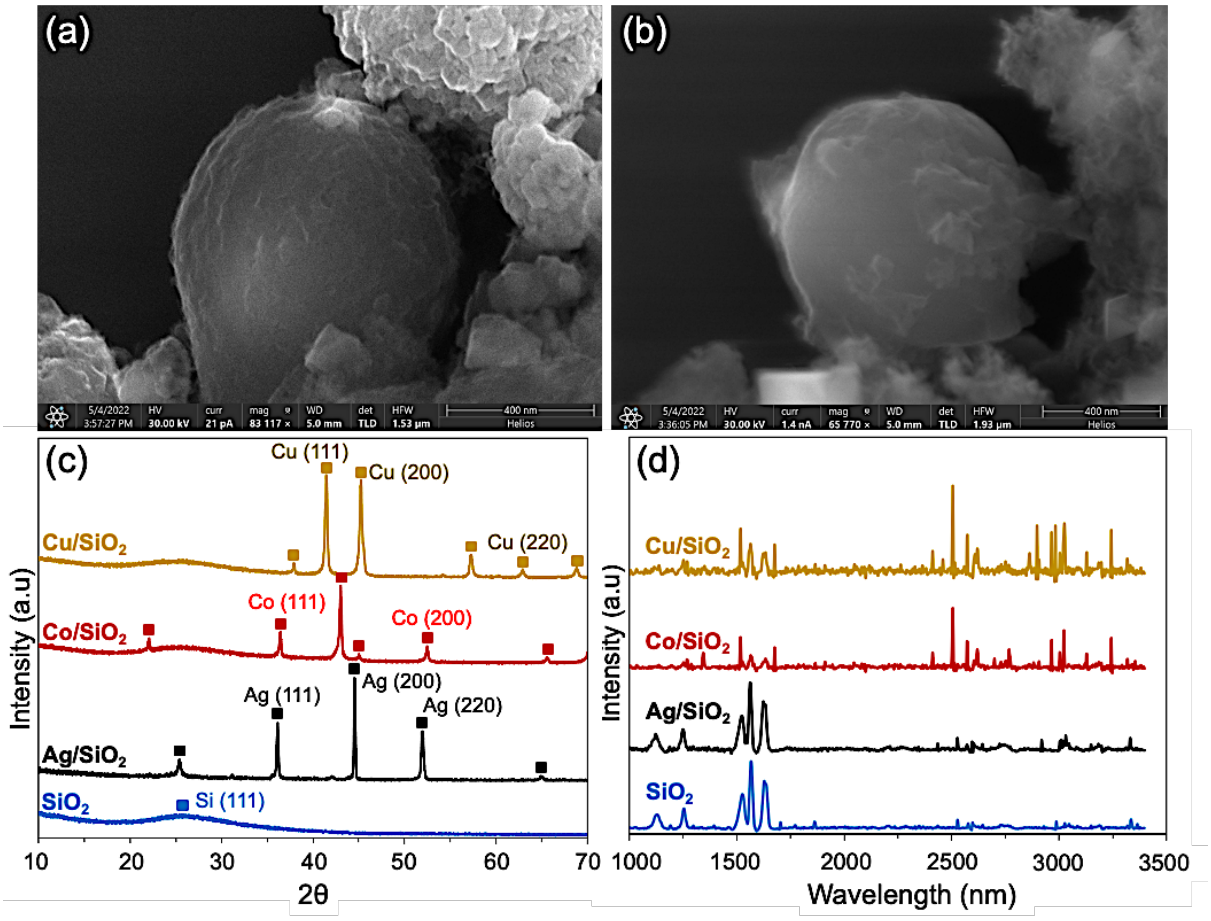

Figure 1. (a) SEM image of the SiO_2 and **(b)** Co/SiO_2; **(c)** XRD patterns and **(d)** Raman spectrum of all prepared catalysts.

Catalytic activity. We studied the catalytic performance by screening the ammonia synthesis rate (r_{NH_3}) over plasma-driven ammonia synthesis from N_2/seawater with various N_2 flowrates i.e., 3.1, 6.2, 12.5, and 25.0 sccm and plasma powers (2, 3, 5, and 6 W) in the absence of catalyst and ammonia was not detected. In contrast, the r_{NH_3} of 0.8 mmol.g_{cat}^{-1}.h^{-1} was obtained from a N_2/H_2 mixture at similar testing conditions (N_2 flowrate was 12.5 sccm and H_2 flowrate was fixed at 12.5 sccm, plasma power of 2 W), which is consistent with our previous studies.[25, 30] This result provides evidence that a catalyst is required for ammonia production from N_2 and seawater. The results for the r_{NH_3} produced from N_2/seawater mixture at different flowrates and plasma powers over the silica sphere catalyst are shown in **Figure 2(a)**. Ammonia synthesis from the N_2/H_2 system (H_2 flowrate was fixed at 12.5 sccm, as shown in (**Figure 2(b)**) over the silica catalyst was also performed to benchmark the catalytic activity. At first, ammonia could

be produced effectively from seawater and N_2 over the SiO_2 catalyst at a relatively low input N_2 flowrate of 3.1 sccm, as shown in **Figure 2(a)**. At this N_2 flowrate and an input plasma power of 2 W, 1.8 mmol.g_{cat}^{-1}.h^{-1} was produced from N_2/seawater system while the highest ammonia synthesis rate could be obtained at the input flowrate of 6.2 sccm with 2.8 mmol.g_{cat}^{-1}.h^{-1}. Noticeably, at similar conditions, the highest ammonia synthesis rate of 2.6 mmol.g_{cat}^{-1}.h^{-1} was also obtained from the N_2/H_2 system with the N_2 flowrate of 3.1 sccm corresponding to the N_2:H_2 ratio of approximately 4.0 (H_2 was fixed at 12.5 sccm), as shown in **Figure 2(b)**. Therefore, at a low plasma input power i.e., 2 W, the N_2/seawater could deliver higher r_{NH_3} that N_2/H_2 system. Further, the increase in the plasma power above 2 W, such as 3W, 5W, and 6 W, led to an enhancement in the ammonia synthesis rate when using N_2/H_2 mixture relative to N_2/seawater (**Figure 2(a)&(b)**). Accordingly, the highest r_{NH_3} value reached was approximately 5.0 mmol.g_{cat}^{-1}.h^{-1}, 1.5 times higher than that produced from N_2/seawater system with 3.2 mmol.g_{cat}^{-1}.h^{-1} at similar plasma power of 6 W. Ammonia could not be detected from the reaction of N_2/seawater in the absence of catalyst, even when varying the plasma power. This result reveals that plasma power has less significant role in ammonia production from N_2/seawater system than that of the catalyst, which played an important factor to secure a desirable ammonia synthesis rate. This show experimentally the importance of the plasma-catalyst synergism when employing sea water as feedstock. Such primary observations reveal novel directions for future work to focus on optimizations for scalable ammonia production from seawater to replace for the use of "gold" hydrogen sustainably. Moreover, the increment in the input flowrates above 6.1 sccm such as 12.5 and 25.0 sccm resulted in the subsequent decline of the r_{NH_3} produced from N_2/seawater. Similarly, r_{NH_3} produced from the N_2/H_2 system also reduced with the rise in input N_2 flowrate (**Figure 2(b)**). The reasons for this observation will be discussed in the next sections. Moreover, the ammonia synthesis rate produced from the N_2/seawater was in range of that obtained over the N_2/pure water system (**Figure S3**) at similar testing conditions and catalysts. As an example, the maximum ammonia

synthesis rate with Co/SiO_2 for pure water was 3.9 $mmol.g_{cat}^{-1}.h^{-1}$ compared to the value obtained for the same catalyst with sea water of 3.7 $mmol.g_{cat}^{-1}.h^{-1}$ at a N_2 flow rate of 6.1 sccm and 2 W. The potential to use seawater instead of pure water is advantageous in a commercial process because of its wide availability. Such observations prove a great potential for further optimization of ammonia production process from N_2 and seawater for industrial scale. Energy yield produced from both N_2/seawater and N_2/H_2 mixtures declined with the increase of input power. Ammonia synthesis from the N_2/seawater at the N_2 input flowrate of 6.2 sccm secured a higher energy yield (2.3 $g_{NH_3}.kW^{-1}.h^{-1}$) than that produced with higher N_2 flowrates such as 12.5 sccm (2.2 $g_{NH_3}.kW^{-1}.h^{-1}$) and 25.0 sccm (0.6 $g_{NH_3}.kW^{-1}.h^{-1}$), as shown in (**Figure 2(c)**. This is because of the high r_{NH_3} obtained at the N_2 input flowrate of 6.2 sccm resulting in better energy yield (Calculation details can be found in Supporting Information). Meanwhile, the highest energy yield gained from ammonia synthesis over the N_2/H_2 mixture was 2.2 $g_{NH_3}.kW^{-1}.h^{-1}$ at a N_2 flowrate of 3.1 sccm (**Figure 2(d)**).

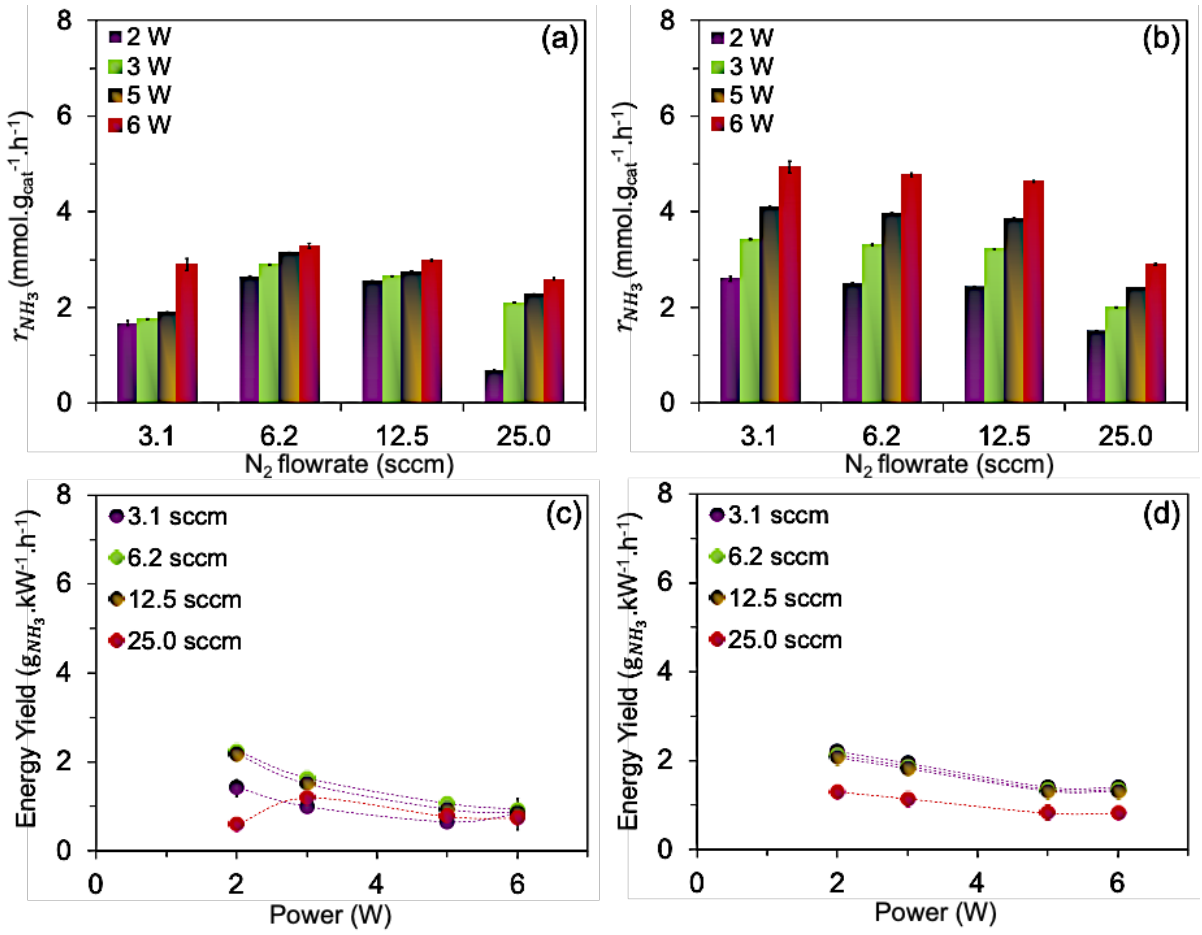

Figure 2. Ammonia synthesis rate (r_{NH_3}) produced from **(a)** N_2/seawater and **(b)** N_2/H_2; Energy yield obtained from **(c)** N_2/seawater and **(d)** N_2/H_2 over the SiO_2 catalyst at different plasma powers.

Such observations further validate the previous assumption that plasma catalytic reactions for ammonia production from N_2/seawater and N_2/H_2 were not solely controlled by the power but by the catalyst as well. In such configuration, the presence of a catalyst in the plasma system appears to alter the plasma-surface reactions, resulting in plasma-catalyst synergism,[50] and by that, promoting the ammonia production. To verify the influence of the metal active centers on ammonia synthesis from N_2/seawater mediated by NTP, this work also employed the SiO_2 as a support to be impregnated with metals such as Ag, Cu, and Co and investigated their catalytic activity. The catalytic performance of these catalysts is shown in **Figure 3**. The presence of a metal supported on the SiO_2 increased the ammonia synthesis rate for the N_2/seawater system significantly. Accordingly, the Co/SiO_2 sample could produce 3.8 $mmol.g_{cat}^{-1}.h^{-1}$ of ammonia while the Ag/SiO_2 and Cu/SiO_2 delivered an ammonia production rate of 3.4 and 3.3 $mmol.g_{cat}^{-1}.h^{-1}$ system with the input N_2 flowrate of 6.2 sccm and power of 2 W, respectively (**Figure 3(a)**). In comparison with other researchers,[33, 34] who have reported to produce ammonia from water, the synthesis rate of 2.67 mmol g_{cat}^{-1} h^{-1} from N_2/water has been observed over the noble catalyst i.e., Ru/MgO at a feed N_2 of 100 sccm and V_{p-p} of 8.23 kV. Our prepared catalysts, Co/SiO_2, displays a comparative performance in terms of ammonia synthesis rate when employing N_2/seawater at a feed N_2 of 6.2 sccm and power of 2 W (about V_{p-p} of 4.12 kV) with a value of 3.7 mmol g_{cat}^{-1} h^{-1}. Moreover, transition metal-based catalysts are highly favourable for large scale application than noble-based catalysts owing to their lower cost and wider availability.[10] Noticeably, the presence of the Co/SiO_2 catalyst in the N_2/H_2 reaction mixture promoted the ammonia synthesis rate (r_{NH_3}) to 6.3 $mmol.g_{cat}^{-1}.h^{-1}$, which is threefold relative to that produced over the SiO_2 catalyst at similar experimental conditions (**Figure 3(b)**). Metallic active centers possessed better activity than oxides like silica, and thereby, delivered better

ammonia production rate.[51] The Co/SiO_2 catalyst displayed highest energy yield of 3.2 and 5.3 $g_{NH_3}.kW^{-1}.h^{-1}$ for ammonia synthesis over the N_2/seawater and N_2/H_2 systems respectively at a power of 2 W (**Figure 3(c) & (d)**). The Ag/SiO_2 and Cu/SiO_2 delivered similar values of energy yield, namely 2.7 and 5.0 $g_{NH_3}.kW^{-1}.h^{-1}$ obtained from the N_2/seawater and N_2/H_2 systems, respectively. Such results confirmed the crucial role of the catalysts in the synthesis of ammonia from the N_2/seawater and N_2/H_2. The Co/SiO_2 catalyst also exhibited the highest ammonia production rate at all testing conditions (**Figure S4**&**S5**). This can be attributed to the lower binding energy of Co with nitrogen relative to the Ag and Cu.[52, 53] Other researchers have also indicated that metals having stronger nitrogen binding energy delivered lower ammonia synthesis rate due to slow N-H formation.[54-56] Accordingly, the theoretical targeted ammonia synthesis yield for an ideal small scale ammonia synthesis processes is 100 $g_{NH_3}.kW^{-1}.h^{-1}$, while the currently reported values employing N_2/H_2 are mostly below 20 $g_{NH_3}.kW^{-1}.h^{-1}$ produced over noble catalysts i.e., Ru-based catalysts [53]. Other catalysts such as Ni or Fe are reported to produce energy yield of below 1.0 $g_{NH_3}.kW^{-1}.h^{-1}$.[57] In comparison with such reported works, the ammonia energy yield obtained from either N_2/seawater (3.2 $g_{NH_3}.kW^{-1}.h^{-1}$) or N_2/H_2 system (5.6 $g_{NH_3}.kW^{-1}.h^{-1}$) over the Co/SiO_2 catalyst in this work displays a competitive performance and high potential for further optimizations.

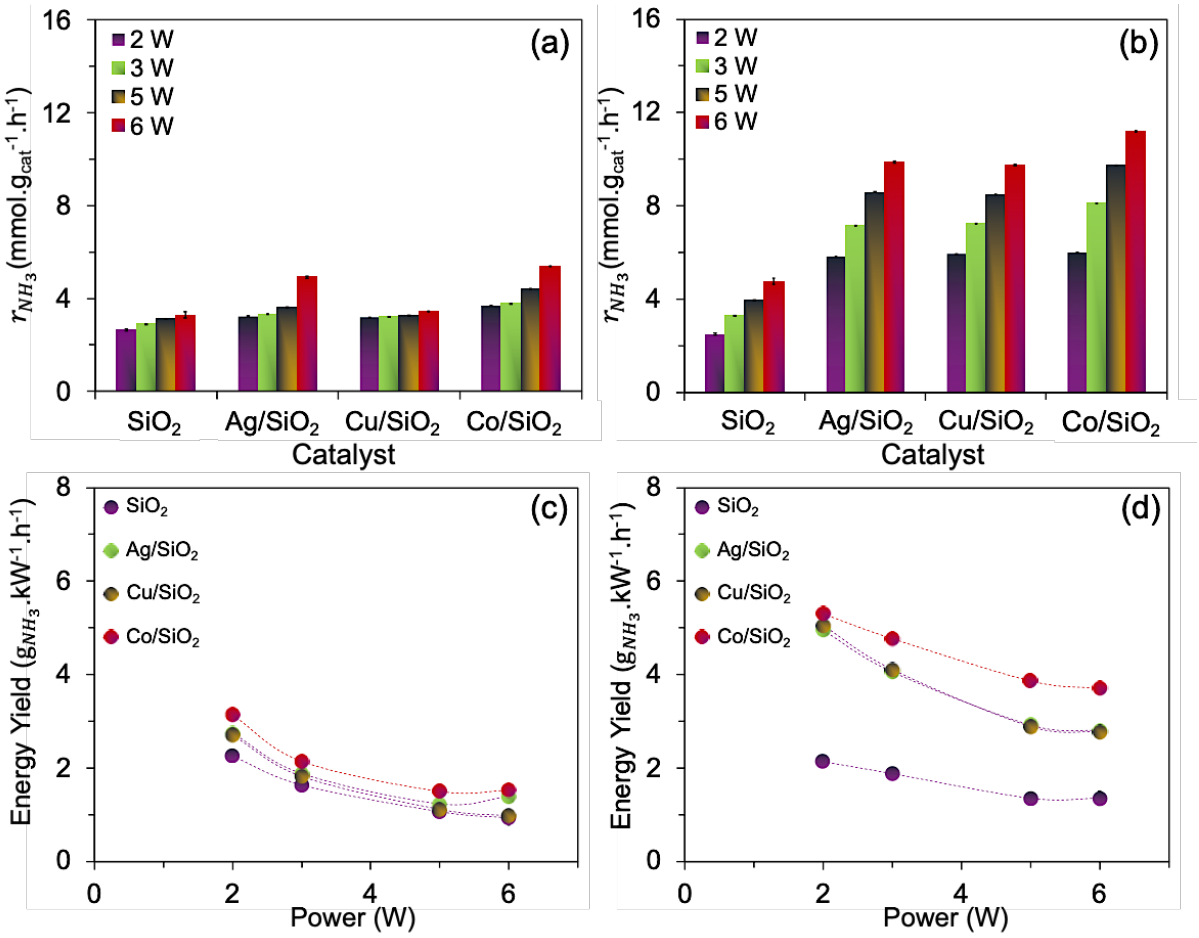

Figure 3. Ammonia synthesis rate (r_{NH_3}) produced from **(a)** N_2/seawater and **(b)** N_2/H_2; Energy yield obtained from ammonia synthesis reaction of **(c)** N_2/seawater and **(d)** N_2/H_2 at different plasma powers and an input N_2 flowrate of 6.2 sccm.

In situ OES. It should be noticed that the inevitable obstacle of the substitution of H_2 by oxygen-contained reactants i.e., seawater is the formation of oxidative species as by-products such as nitrogen oxides. In this work, operando optical emission spectroscopy (OES) analysis was performed to study the plasma excitation process with and without catalyst. The results are shown in **Figure 4.** The overall OES spectrum for ammonia synthesis from different routes are well-detected (**Figure 4(a)**). Noticeably, the main nitrogen oxide product detected was nitrous oxide (N_2O), as shown in (**Figure 4(b)**). Other nitrogen oxides such as N_xO_y were possibly generated but within concentrations below detection limits. Compared with the plasma-only experiments, the catalyst plasma experiment for ammonia synthesis from N_2 and seawater exhibited insignificant differences in the intensity of the N_2O-related peaks (**Figure**

4(b)). However, its intensity was higher than that of the ammonia synthesis route from N_2 and H_2. Such observations indicate that N_2O formation occurs predominantly in the gas phase and is promoted with the presence of seawater. Another possible reason for the formation of nitrogen oxide that cannot be neglected is the role of interstitial oxygen in the silica catalyst. Whereby, such lattice oxygen generates transient vacancies and replenish from the gas-phase oxygen source to combine with vibrationally excited nitrogen adatoms on the silica surface, and thereby, enhances the formation of nitrogen oxide.[58] Noticeably, NH_x-assigned peak at 336.1 nm was well-detected from the plasma catalyst processes with N_2/H_2 and N_2/seawater while it missed from the plasma-only process with N_2/seawater (**Figure 4(c)**). This result validates the absence of ammonia product from N_2/seawater over the plasma-only route detected from GC as discussed previously. In addition, plasma-activated nitrogen species exist in the form of vibrational and rotational excitation, electronic excitation, and ionization without dissociation being observed (**Figure 4(d)**).

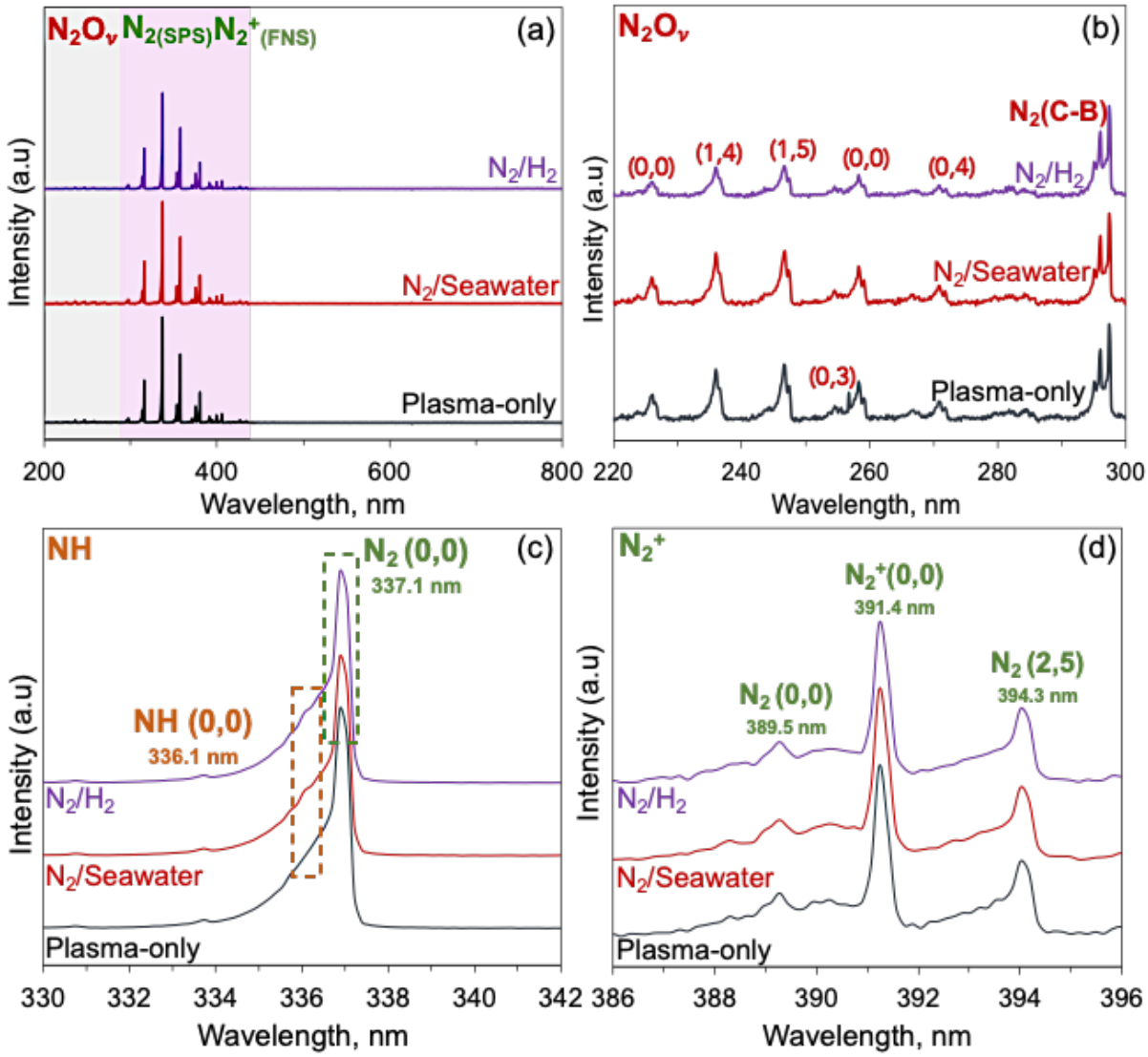

Figure 4. (a) Overall OES spectrum (200-800 nm) for plasma-assisted catalytic ammonia synthesis from N_2/H_2, N_2/seawater, and plasma without catalyst (plasma-only) of ammonia synthesis reaction from N_2/seawater; **(b)** zoom-in OES spectrum of $NO_{(v)}$ (220-300 nm); **(c)** zoom-in OES spectrum of NH (330-342 nm); and **(d)** zoom-in OES spectrum of N_2^+ (386-396 nm) obtained over the Co/SiO_2 catalyst.

Noticeably, the OES spectrum collected from the ammonia synthesis reactions over the Co/SiO_2 catalyst (**Figure 5**) well displayed the presence of N_2O, which is similar to that obtained over the SiO_2 catalyst. Meanwhile, nitrous oxides were not detected from the reaction over the Ag/SiO_2. By experimental data and computational calculations, Kepp et al.,[59] have indicated that metal-oxygen interactions are in an order of Co, Cu, and Ag with bond

dissociation enthalpy with oxygen of 420, 310, and 200 kJ/mol, respectively. Given stronger affinity to oxygen, more active oxygen was absorbed on the Co/SiO_2 surface and reacted with N_2^* to form nitrous oxide while the reactions occurred over the Cu/SiO_2 presented weak intensity of nitrous oxide, as shown in **Figure 5**. For the metals with weaker affinity such as Ag or Cu, active oxygen was possibly prone to recombination with H atoms. These conclusions can be verified via the selectivity of N_2O and NH_3 (**Figure S6**). The N_2O calibration curve is also shown in **Figure S7**. At a N_2 input flowrate of 6.2 sccm and 6 W, the Ag/SiO_2 and Co/SiO_2 catalysts displayed lower N_2O selectivity of 27.5 and 32.0%, respectively than that of the SiO_2 and the Cu/SiO_2, which produced the N_2O selectivity of 47.6 and 41.8%, respectively (**Eq.(3)**, Supporting Information).

In term of nitrogen fixation, such nitrogen oxide can be used as a useful product for other chemicals production. A possible concept to make a full use of downstream products from ammonia synthesis is the addition of a membrane DBD plasma reactor to separate produced N_2O for other chemical synthesis i.e., HNO_3 with air while the formed ammonia can be liquefied. This product separation strategy in a DBD reactor has been explored by our group for the N_2/H_2 plasma ammonia synthesis.[25] Another solution is to recycle formed NO_x to the reactor for ammonia synthesis.[60]A possible concern is whether a desalination step is necessary to translate seawater to purer water prior to entering to the DBD reactor for ammonia synthesis reaction. This is originated from an apprehension that seawater possibly causes oxidation of the electrode of the DBD reactor. Nevertheless, even though either pure water or air was used, the inner electrode of the DBD reactor also deals with oxidative issues under long-term cycling reactions. Such phenomenon requires a thoughtful study to assess the effects of oxygen-consisted co-reactants such as pure water, seawater, or air, which is out of the main scope of this work. While experimental results of this work indicated insignificant difference of ammonia production rate from both N_2/pure water and N_2/seawater, the addition of such desalination step into the process undoubtedly raises investment capital. Future work in this

area can focus on the development of highly active catalysts, process optimization, and evaluation of scale-up capacity with a vision to propose a feasible technology for ammonia production plants at harbours or remote sea areas.

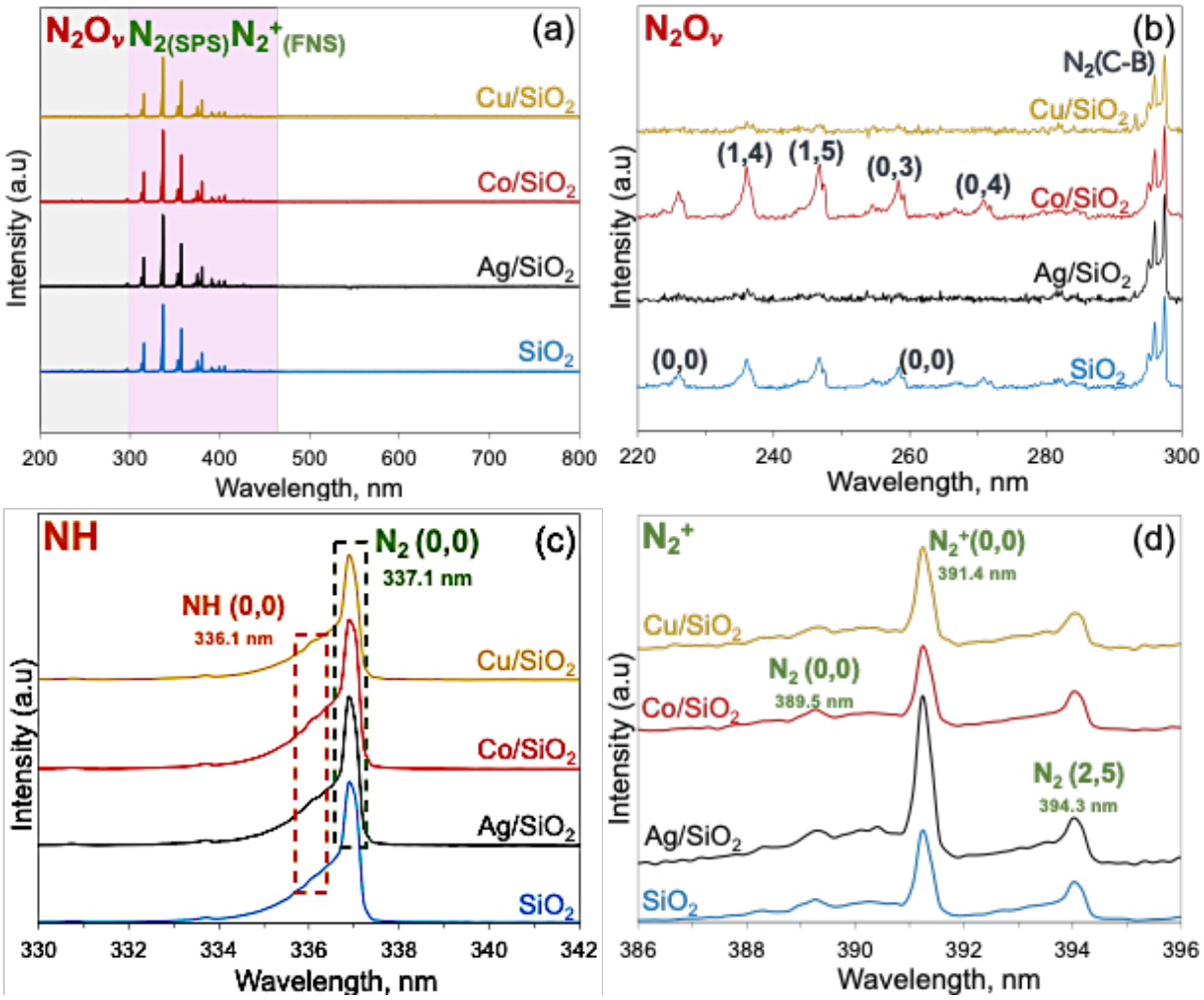

Figure 5. (a) Overall OES spectrum (200-800 nm) for plasma-assisted catalytic ammonia synthesis from N_2/seawater, **(b)** zoom-in OES spectrum of $NO_{(\gamma)}$ (220-300 nm); **(c)** zoom-in OES spectrum of NH (330-342 nm); and **(d)** zoom-in OES spectrum of N_2^+ (386-396 nm) of different catalysts. The OES spectrum of the SiO_2 catalyst is re-presented for comparison purpose.

Mechanistic insights of seawater and N_2 plasma activation for ammonia production. Despite the recent developments and progresses in plasma-mediated ammonia synthesis from N_2 and H_2, few efforts have been made to study the reaction mechanism of these reactions.[24, 61, 62] Meanwhile, the use of novel hydrogen sources such as seawater is expected to alter the

reaction pathways.[63] This work seeks to provide mechanistic insights into the plasma activation of N_2 and seawater for ammonia production. Such premises are significantly important for subsequent research on the optimization of ammonia synthesis from seawater and N_2 sustainably. Experimental results of this work indicated that ammonia was not detected from the reaction between N_2 and seawater. Therefore, it is worthwhile to mention that a catalyst is needed to provide an active surface for absorbed active N_2 species to react with H* species dissociated from H_2O (seawater). Other researchers also reveal that an active surface is necessary to secure a good ammonia synthesis rate. [57] Since even if the DBD plasma offers a high degree of excitation (either vibrational or electronic) it observes a low degree of dissociation.[64] Researchers also indicate that N_2 is not completely dissociated in the plasma environment and the presence of a heterogeneous catalyst facilitates the dissociation of the plasma-generated species.[51] The well-reported mechanisms for ammonia synthesis from N_2 and H_2 includes the formation of plasma-induced vibrationally excited $N_{2(v)}$ species and the excitation of adsorbed $N_{(ads)}$ on the catalyst surface to react with H_2 to form NH_3 *via* either Eley-Rideal (E-R) or Langmuir-Hinshelwood (L-H).[23, 62, 65-68] Both the E-R and L-H mechanisms are involved in many reactions to form ammonia. The presence of seawater alters such mechanisms by adding the excitation and/or ionization of water molecules. Zhou and co-workers[33] proposed a detailed mechanism on plasma assisted N_2 and pure water reaction for ammonia synthesis. Nevertheless, we postulate that the dissociation of water-plasma interface cannot be neglected. A schematic diagram describing the possible reaction pathway for ammonia synthesis from N_2 and seawater is shown in **Figure 6**. In the N_2/seawater system, H_2O (seawater) molecules participate in the reaction in two ways. The first is by being mixed with N_2 and being vibrationally excited by plasma in the gaseous phase. These excited species are subsequently adsorbed on the silica catalyst surface followed by their dissociation. Surface reactions under plasma regime occur and produce ammonia *via* either E-R or L-H mechanisms as discussed early in our previous works on the N_2/H_2 system. Then the nitrogen plasma jet

reacts with H_2O (seawater) to generate NH and OH radicals.[69] Therefore, the ammonia production from the N_2/seawater system involved reactions between H_2O (seawater) molecules and excited N_2 species in the plasma and on the catalyst surface. The excitation of N_2 mainly occurs in the gaseous phase while the formation of H and OH species are prevalent at the interface between the gaseous and humid phase (seawater), where the combination of NH and H occurs to form ammonia. At the outermost layer of the H_2O (seawater) molecule, H could be produced through plasma-water interactions. Therefore, the extraction of H from water molecules plays an important role in the formation of ammonia. This deduction is in good agreement with other researchers.[70, 71] A stronger dissociation of H_2O (seawater) to form H species is expected to enhance the ammonia synthesis rate. Given the short life span of active H species, the large accumulation of H secures the higher ammonia synthesis rate. However, experimental results in this work show a reduction in ammonia production rate at the input N_2 flowrates higher than 6.2 sccm such as 12.5 sccm or 25 sccm (**Figure 2** and **Figure S8**). This result is possibly due to the presence of a larger amount of H_2O (humid seawater) by the higher N_2 sweep flowrate, which possibly led to an excessive surface coverage of steam/ OH adatoms, and thereby, resulting in a significant reduction in activity of the silica catalyst. Commonly accompanied by a highly negative reaction order for hydrogen (-1) when a catalyst surface is excessively covered.[72] Moreover, H_2O (seawater) vapor cause the quenching of N_2 vibrational levels given the N_2/H_2O vibrational-translational relaxation, which induce the strong electron dissociative attachment to molecules, reducing electron density, and thereby, reducing ammonia synthesis rate.[73] The larger presence of seawater resulted in the higher formation of N_2O originated from the reaction of O* and N_2*, which reduced the production of ammonia given less available N_2* to react with H to form NH. It cannot be neglected that OH* was generated from the dissociation of H_2O molecules. Nevertheless, the presence of such OH* species would lead to the formation of H_2O_2,[74] which was not detected from this work. Therefore, such hydroxyl radicals with significant short life could get dissociated to H* and

O* subsequently. These criteria can be fulfilled by adding an active metal/metallic alloy centres on the silica support. Experimental results in this work also indicated that even if the Co/SiO_2 catalyst displayed the highest ammonia synthesis rate, a strongest N_2O-related spectra was detected. While the Ag/SiO_2 catalyst displayed no OES spectra of NO_x species but showed a competitive activity relative to the Co/SiO_2, as discussed previously. Hence, future work can focus on enhancement of the catalytic activity of oxygen-phobic metals or electron density on the catalyst surface to dissociate N_2 and maintain relatively weak intermediate bindings effectively. Such active metals would be ideal if they possess high affinity to oxidative oxygen species to offer strong bindings or act as oxygen sinks[75, 76] to hinder the formation of nitrogen oxide.

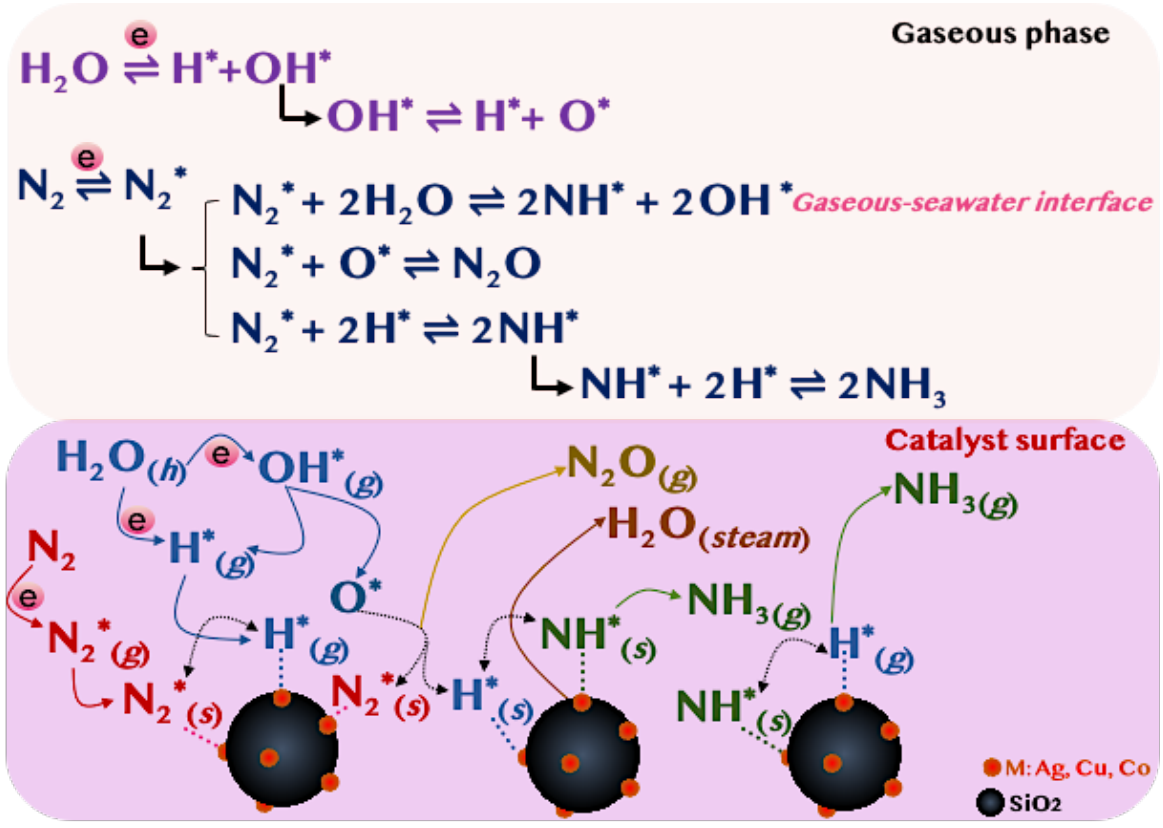

Figure 6. Schematic diagram of plasma-driven ammonia synthesis from N_2 and seawater over the metallic supported on SiO_2.

CONCLUSIONS

In this work, ammonia was successfully produced from N_2 and seawater at ambient conditions directly from using renewable sources such as N_2, seawater, and electricity potentially from

solar or wind. The presence of a catalyst was required to secure the formation of ammonia from the N_2/seawater and an ammonia synthesis rate of 2.8 mmol.g_{cat}^{-1}.h^{-1} and an energy efficiency of 2.3 $g_{NH_3}.kW^{-1}.h^{-1}$could be produced from N_2/seawater reaction with a N_2 flowrate of 6.2 sccm and a relatively low plasma input power of 2 W over the SiO_2. The metals supported on SiO_2 such as Ag/SiO_2, Cu/SiO_2 and Co/SiO_2 enhanced the ammonia production rate and energy yield significantly. The use of seawater as an alternative H_2 source delivered a comparative ammonia production rate and energy yield relative to the utilization of pure H_2. Plasma power has a less significant role in ammonia production relative to the catalyst that acted as an important factor to secure a desirable ammonia synthesis rate. This work has opened novel research directions for future work to rationally design active metals supported on silica or other good dielectric materials like perovskites for ammonia production from seawater sustainably and economically.

ASSOCIATED CONTENT

Supporting Information

The Supporting Information is available free of charge on the ACS Publications website at DOI: [xxx]. Location of seawater collection, Schematic diagram of the experimental setup; Calculation details; Ammonia synthesis rate for SiO_2 and Co/SiO_2 for N_2/pure water; Ammonia synthesis rate for prepared catalysts over different flow rate and powers; Energy Yield for prepared catalysts over different flow rate and powers; NH_3 and N_2O selectivity; N_2O calibration curve; Ammonia synthesis rate and energy yield obtained over the prepared catalyst at different flowrates and powers.

AUTHOR INFORMATION

Corresponding Author

*Maria L. Carreon - Mechanical Engineering Department, University of Massachusetts Lowell, One University Avenue, Lowell, Massachusetts 01854-5043, USA; ORCID: orcid.org/0000-0002-2717-1577; E-mail: Maria_Carreon@uml.edu

Author

Hoang M. Nguyen - Mechanical Engineering Department, University of Massachusetts Lowell, One University Avenue, Lowell, Massachusetts 01854-5043, USA; ORCID: orcid.org/0000-0002-3730-1267.

Fnu Gorky - Mechanical Engineering Department, University of Massachusetts Lowell, One University Avenue, Lowell, Massachusetts 01854-5043, USA.

Shelby Guthrie - Mechanical Engineering Department, University of Massachusetts Lowell, One University Avenue, Lowell, Massachusetts 01854-5043, USA.

Notes

The authors declare no competing financial interest.

ACKNOWLEDGEMENTS

Maria L. Carreon acknowledges the support from NSF CBET Award No. 2203166 and grant No. DE-SC0023261, U.S. DEPARTMENT OF ENERGY, Basic Research.

REFERENCES

(1) Ye, L.; Li, H.; Xie, K., Sustainable ammonia production enabled by membrane reactor. *Nat. Sustain.* **2022**, https://doi.org/10.1038/s41893-022-00908-6.

(2) Jeerh, G.; Zhang, M.; Tao, S., Recent progress in ammonia fuel cells and their potential applications. *J. Mater. Chem. A* **2021,** *9* (2), 727-752, https://doi.org/10.1039/D0TA08810B.

(3) Kim, J.; Huh, C.; Seo, Y., End-to-end value chain analysis of isolated renewable energy using hydrogen and ammonia energy carrier. *Energy Convers. Manag.* **2022,** *254*, 115247, https://doi.org/10.1016/j.enconman.2022.115247.

(4) Kang, D. W.; Holbrook, J. H., Use of NH_3 fuel to achieve deep greenhouse gas reductions from US transportation. *Energy Rep.* **2015,** *1*, 164-168, https://doi.org/10.1016/j.egyr.2015.08.001.

(5) Xu, X.; Liu, E.; Zhu, N.; Liu, F.; Qian, F., Review of the current status of ammonia-blended hydrogen fuel engine development. *Energies.* **2022,** *15* (3), 1023, https://doi.org/10.3390/en15031023.

(6) Kurien, C.; Mittal, M., Review on the production and utilization of green ammonia as an alternate fuel in dual-fuel compression ignition engines. *Energy Convers. Manag.* **2022,** *251*, 114990, https://doi.org/10.1016/j.enconman.2021.114990.

(7) Liu, Y.; Wang, C. W.; Xu, X. F.; Liu, B. W.; Zhang, G. M.; Liu, Z. W.; Chen, Q.; Zhang, H. B., Synergistic effect of Co–Ni bimetal on plasma catalytic ammonia synthesis. *Plasma Chem. Plasma Process.* **2022,** *42* (2), 267-282, https://doi.org/10.1007/s11090-021-10223-1.

(8) Zhu, X.; Liu, J.; Hu, X.; Zhou, Z.; Li, X.; Wang, W.; Wu, R.; Tu, X., Plasma-catalytic synthesis of ammonia over Ru-based catalysts: Insights into the support effect. *J. Energy Inst.* **2022,** *102*, 240-246, https://doi.org/10.1016/j.joei.2022.02.014.

(9) Zhao, H.; Song, G.; Chen, Z.; Yang, X.; Yan, C.; Abe, S.; Ju, Y.; Sundaresan, S.; Koel, B. E., In situ identification of NNH and N_2H_2 by using molecular-beam mass spectrometry in plasma-assisted catalysis for NH_3 synthesis. *ACS Energy Lett.* **2022,** *7* (1), 53-58, https://doi.org/10.1021/acsenergylett.1c02207.

(10) Nguyen, H. M.; Sunarso, J.; Li, C.; Pham, G. H.; Phan, C.; Liu, S., Microwave-assisted catalytic methane reforming: A review. *Appl. Catal., A.* **2020,** *599*, 117620, https://doi.org/10.1016/j.apcata.2020.117620.

(11) Oni, A.; Anaya, K.; Giwa, T.; Di Lullo, G.; Kumar, A., Comparative assessment of blue hydrogen from steam methane reforming, autothermal reforming, and natural gas decomposition technologies for natural gas-producing regions. *Energy Convers. Manag.* **2022,** *254*, 115245, https://doi.org/10.1016/j.enconman.2022.115245.

(12) Sun, J.; Alam, D.; Daiyan, R.; Masood, H.; Zhang, T.; Zhou, R.; Cullen, P. J.; Lovell, E. C.; Jalili, A. R.; Amal, R., A hybrid plasma electrocatalytic process for sustainable ammonia production. *Energy Environ. Sci.* **2021,** *14* (2), 865-872, https://doi.org/10.1039/D0EE03769A.

(13) Oliver, E. C.; Donat, M. G.; Burrows, M. T.; Moore, P. J.; Smale, D. A.; Alexander, L. V.; Benthuysen, J. A.; Feng, M.; Sen Gupta, A.; Hobday, A. J., Longer and more frequent marine heatwaves over the past century. *Nat. Commun.* **2018,** *9* (1), 1-12, https://doi.org/10.1038/s41467-018-03732-9.

(14) Hawtof, R.; Ghosh, S.; Guarr, E.; Xu, C.; Mohan Sankaran, R.; Renner, J. N., Catalyst-free, highly selective synthesis of ammonia from nitrogen and water by a plasma electrolytic system. *Sci. Adv* **2019,** *5* (1), eaat5778, https://doi.org/10.1126/sciadv.aat5778.

(15) Zheng, J.; Lyu, Y.; Qiao, M.; Wang, R.; Zhou, Y.; Li, H.; Chen, C.; Li, Y.; Zhou, H.; Wang, S., Photoelectrochemical synthesis of ammonia on the aerophilic-hydrophilic heterostructure with 37.8% efficiency. *Chem* **2019,** *5* (3), 617-633, https://doi.org/10.1016/j.chempr.2018.12.003.

(16) Patel, H.; Sharma, R. K.; Kyriakou, V.; Pandiyan, A.; Welzel, S.; van de Sanden, M. C. M.; Tsampas, M. N., Plasma-activated electrolysis for cogeneration of nitric oxide and hydrogen from water and nitrogen. *ACS Energy Lett.* **2019,** *4* (9), 2091-2095, https://doi.org/10.1021/acsenergylett.9b01517.

(17) Sharma, R. K.; Patel, H.; Mushtaq, U.; Kyriakou, V.; Zafeiropoulos, G.; Peeters, F.; Welzel, S.; van de Sanden, M. C. M.; Tsampas, M. N., Plasma activated electrochemical ammonia synthesis from nitrogen and water. *ACS Energy Lett.* **2021,** *6* (2), 313-319, https://doi.org/10.1021/acsenergylett.0c02349.

(18) Zhou, Z.; Pei, Z.; Wei, L.; Zhao, S.; Jian, X.; Chen, Y., Electrocatalytic hydrogen evolution under neutral pH conditions: current understandings, recent advances, and future prospects. *Energy Environ. Sci.* **2020,** *13* (10), 3185-3206, https://doi.org/10.1039/D0EE01856B.

(19) Peng, P.; Schiappacasse, C.; Zhou, N.; Addy, M.; Cheng, Y.; Zhang, Y.; Ding, K.; Wang, Y.; Chen, P.; Ruan, R., Sustainable non-thermal plasma-assisted nitrogen fixation—synergistic catalysis. *ChemSusChem* **2019,** *12* (16), 3702-3712, https://doi.org/10.1002/cssc.201901211.

(20) Sun, Y.; Wu, J.; Wang, Y.; Li, J.; Wang, N.; Harding, J.; Mo, S.; Chen, L.; Chen, P.; Fu, M.; Ye, D.; Huang, J.; Tu, X., Plasma-catalytic CO_2 hydrogenation over a Pd/ZnO catalyst: In situ probing of gas-phase and surface reactions. *JACS Au* **2022**, https://doi.org/10.1021/jacsau.2c00028.

(21) Chen, G.; Tu, X.; Homm, G.; Weidenkaff, A., Plasma pyrolysis for a sustainable hydrogen economy. *Nat. Rev. Mater* **2022,** *7* (5), 333-334, https://doi.org/10.1038/s41578-022-00439-8.

(22) Sun, J.; Alam, D.; Daiyan, R.; Masood, H.; Zhang, T.; Zhou, R.; Cullen, P. J.; Lovell, E. C.; Jalili, A.; Amal, R., A hybrid plasma electrocatalytic process for sustainable ammonia production. *Energy Environ. Sci.* **2021,** *14* (2), 865-872, https://doi.org/10.1039/D0EE03769A.
(23) Rouwenhorst, K. H. R.; Burbach, H. G. B.; Vogel, D. W.; Núñez Paulí, J.; Geerdink, B.; Lefferts, L., Plasma-catalytic ammonia synthesis beyond thermal equilibrium on Ru-based catalysts in non-thermal plasma. *Catal. Sci. Technol* **2021,** *11* (8), 2834-2843, https://doi.org/10.1039/D0CY02189J.
(24) Wang, Y.; Craven, M.; Yu, X.; Ding, J.; Bryant, P.; Huang, J.; Tu, X., Plasma-enhanced catalytic synthesis of ammonia over a Ni/Al_2O_3 catalyst at near-room temperature: Insights into the importance of the catalyst surface on the reaction mechanism. *ACS. Catal.* **2019,** *9* (12), 10780-10793, https://doi.org/10.1021/acscatal.9b02538.
(25) Gorky, F.; Nguyen, H. M.; Lucero, J. M.; Guthrie, S.; Crawford, J. M.; Carreon, M. A.; Carreon, M. L., CC3 porous organic cage crystals and membranes for the non-thermal plasma catalytic ammonia synthesis. *Chem. Eng. J. Adv.* **2022**, 100340, https://doi.org/10.1016/j.ceja.2022.100340.
(26) Nguyen, H. M.; Carreon, M. L., Non-thermal plasma-assisted deconstruction of high-density polyethylene to hydrogen and light hydrocarbons over hollow ZSM-5 microspheres. *ACS Sustain. Chem. Eng.* **2022,** *10* (29), 9480-9491, https://doi.org/10.1021/acssuschemeng.2c01959.
(27) Gershman, S.; Fetsch, H.; Gorky, F.; Carreon, M. L., Identifying regimes during plasma catalytic ammonia synthesis. *Plasma Chem. Plasma Process.* **2022,** *42* (4), 731-757, https://doi.org/10.1007/s11090-022-10258-y.
(28) Gorky, F.; Lucero, J. M.; Crawford, J. M.; Blake, B.; Carreon, M. A.; Carreon, M. L., Plasma-induced catalytic conversion of nitrogen and hydrogen to ammonia over zeolitic imidazolate frameworks ZIF-8 and ZIF-67. *ACS Appl. Mater. Interfaces* **2021,** *13* (18), 21338-21348, https://doi.org/10.1021/acsami.1c03115.
(29) Gorky, F.; Lucero, J. M.; Crawford, J. M.; Blake, B. A.; Guthrie, S. R.; Carreon, M. A.; Carreon, M. L., Insights on cold plasma ammonia synthesis and decomposition using alkaline earth metal-based perovskites. *Catal. Sci. Technol* **2021,** *11* (15), 5109-5118, https://doi.org/10.1039/D1CY00729G.
(30) Gorky, F.; Best, A.; Jasinski, J.; Allen, B. J.; Alba-Rubio, A. C.; Carreon, M. L., Plasma catalytic ammonia synthesis on Ni nanoparticles: The size effect. *J. Catal.* **2021,** *393*, 369-380, https://doi.org/10.1016/j.jcat.2020.11.030.
(31) Shah, J. R.; Gorky, F.; Lucero, J.; Carreon, M. A.; Carreon, M. L., Ammonia synthesis via atmospheric plasma catalysis: Zeolite 5A, a case of study. *Ind. Eng. Chem. Res.* **2020,** *59* (11), 5167-5176, https://doi.org/10.1021/acs.iecr.9b05220.
(32) Shah, J.; Gorky, F.; Psarras, P.; Seong, B.; Gómez-Gualdrón, D. A.; Carreon, M. L., Enhancement of the yield of ammonia by hydrogen-sink effect during plasma catalysis. *ChemCatChem.* **2020,** *12* (4), 1200-1211, https://doi.org/10.1002/cctc.201901769.
(33) Zhang, T.; Zhou, R.; Zhang, S.; Zhou, R.; Ding, J.; Li, F.; Hong, J.; Dou, L.; Shao, T.; Murphy, A. B.; Ostrikov, K.; Cullen, P. J., Sustainable ammonia synthesis from nitrogen and water by one-step plasma catalysis. *Energy Environ. Mat. n/a* (n/a), https://doi.org/10.1002/eem2.12344.
(34) Hong, J.; Zhang, T.; Zhou, R.; Zhang, S.; Dou, L.; Zhou, R.; Ashford, B.; Shao, T.; Murphy, A.; Ostrikov, K.; Cullen, P. J., Green chemical pathway of plasma synthesis of ammonia from nitrogen and water: a comparative kinetic study with N_2/H_2 system. *Green Chem.* **2022**, https://doi.org/10.1039/D2GC02299K.
(35) Hess, C.; Schlögl, R., *Nanostructured catalysts: selective oxidations*. Royal Society of Chemistry: 2011; https://doi.org/10.1039/9781847559876.
(36) Suttikul, T.; Sreethawong, T.; Sekiguchi, H.; Chavadej, S., Ethylene epoxidation over alumina- and silica-supported silver catalysts in low-temperature AC dielectric barrier

discharge. *Plasma Chem. Plasma Process.* **2011,** *31* (2), 273-290, https://doi.org/10.1007/s11090-010-9280-1.

(37) Norby, T.; Widerøe, M.; Glöckner, R.; Larring, Y., Hydrogen in oxides. *Dalton Trans.* **2004,** (19), 3012-3018, https://doi.org/10.1039/B403011G.

(38) Wannagat, U., The silicon-nitrogen bond. In *Biochemistry of Silicon and Related Problems*, Bendz, G.; Lindqvist, I.; Runnström-Reio, V., Eds. Springer US: Boston, MA, 1978; pp 77-90, https://doi.org/10.1007/978-1-4613-4018-8_3.

(39) Gorky, F.; Guthrie, S. R.; Smoljan, C. S.; Crawford, J. M.; Carreon, M. A.; Carreon, M. L., Plasma ammonia synthesis over mesoporous silica SBA-15. *J. Phys. D: Appl. Phys* **2021,** *54* (26), 264003, https://doi.org/10.1088/1361-6463/abefbc.

(40) Choi, H. M.; Lee, S.-J.; Moon, S.-H.; Phan, T. N.; Jeon, S. G.; Ko, C. H., Comparison between unsupported mesoporous Co_3O_4 and supported Co_3O_4 on mesoporous silica as catalysts for N_2O decomposition. *Catal. Commun.* **2016,** *82*, 50-54, https://doi.org/10.1016/j.catcom.2016.04.022.

(41) Piumetti, M.; Hussain, M.; Fino, D.; Russo, N., Mesoporous silica supported Rh catalysts for high concentration N_2O decomposition. *Appl. Catal., B* **2015,** *165*, 158-168, https://doi.org/10.1016/j.apcatb.2014.10.008.

(42) Zhu, H.; Mao, Z.; Liu, B.; Yang, T.; Feng, X.; Jin, H.; Peng, C.; Yang, C.; Wang, J.; Fang, X., Regulating catalyst morphology to boost the stability of Ni–Mo/Al_2O_3 catalyst for ebullated-bed residue hydrotreating. *Green Energy Environ.* **2021,** *6* (2), 283-290, https://doi.org/10.1016/j.gee.2020.05.001.

(43) Pagis, C.; Morgado Prates, A. R.; Farrusseng, D.; Bats, N.; Tuel, A., Hollow zeolite structures: an overview of synthesis methods. *Chem. Mater.* **2016,** *28* (15), 5205-5223, https://doi.org/10.1021/acs.chemmater.6b02172.

(44) Yoo, W. C.; Kumar, S.; Wang, Z.; Ergang, N. S.; Fan, W.; Karanikolos, G. N.; McCormick, A. V.; Penn, R. L.; Tsapatsis, M.; Stein, A., Nanoscale reactor engineering: hydrothermal synthesis of uniform zeolite particles in massively parallel reaction chambers. *Angew. Chem.* **2008,** *120* (47), 9236-9239, https://doi.org/10.1002/anie.200803103.

(45) Taghvaei, H.; Moaddeli, A.; Khalafi-Nezhad, A.; Iulianelli, A., Catalytic hydrodeoxygenation of lignin pyrolytic-oil over Ni catalysts supported on spherical Al-MCM-41 nanoparticles: Effect of Si/Al ratio and Ni loading. *Fuel.* **2021,** *293*, 120493, https://doi.org/10.1016/j.fuel.2021.120493.

(46) Skuja, L.; Güttler, B.; Schiel, D.; Silin, A. R., Quantitative analysis of the concentration of interstitial O_2 molecules in SiO_2 glass using luminescence and Raman spectrometry. *J. Appl. Phys* **1998,** *83* (11), 6106-6110, https://doi.org/10.1063/1.367480.

(47) Agnello, S.; Francesca, D. D.; Alessi, A.; Iovino, G.; Cannas, M.; Girard, S.; Boukenter, A.; Ouerdane, Y., Interstitial O_2 distribution in amorphous SiO_2 nanoparticles determined by Raman and photoluminescence spectroscopy. *J. Appl. Phys* **2013,** *114* (10), 104305, https://doi.org/10.1063/1.4820940.

(48) Kajihara, K.; Miura, T.; Kamioka, H.; Aiba, A.; Uramoto, M.; Morimoto, Y.; Hirano, M.; Skuja, L.; Hosono, H., Diffusion and reactions of interstitial oxygen species in amorphous SiO_2: A review. *J. Non-Cryst. Solids.* **2008,** *354* (2), 224-232, https://doi.org/10.1016/j.jnoncrysol.2007.07.038.

(49) Ivanda, M.; Clasen, R.; Hornfeck, M.; Kiefer, W., Raman spectroscopy on SiO_2 glasses sintered from nanosized particles. *J. Non-Cryst. Solids.* **2003,** *322* (1), 46-52, https://doi.org/10.1016/S0022-3093(03)00172-8.

(50) Wang, Y.; Yang, W.; Xu, S.; Zhao, S.; Chen, G.; Weidenkaff, A.; Hardacre, C.; Fan, X.; Huang, J.; Tu, X., Shielding protection by mesoporous catalysts for improving plasma-catalytic ambient ammonia synthesis. *J. Am. Chem. Soc* **2022**, https://doi.org/10.1021/jacs.2c01950.

(51) Patil, B. S.; Cherkasov, N.; Srinath, N. V.; Lang, J.; Ibhadon, A. O.; Wang, Q.; Hessel, V., The role of heterogeneous catalysts in the plasma-catalytic ammonia synthesis. *Catal. Today* **2021,** *362*, 2-10, https://doi.org/10.1016/j.cattod.2020.06.074.
(52) Mehta, P.; Barboun, P.; Herrera, F. A.; Kim, J.; Rumbach, P.; Go, D. B.; Hicks, J. C.; Schneider, W. F., Overcoming ammonia synthesis scaling relations with plasma-enabled catalysis. *Nat. Catal.* **2018,** *1* (4), 269-275, https://doi.org/10.1038/s41929-018-0045-1.
(53) Rouwenhorst, K. H. R.; Engelmann, Y.; van 't Veer, K.; Postma, R. S.; Bogaerts, A.; Lefferts, L., Plasma-driven catalysis: green ammonia synthesis with intermittent electricity. *Green Chem.* **2020,** *22* (19), 6258-6287, https://doi.org/10.1039/D0GC02058C.
(54) Foster, S. L.; Bakovic, S. I. P.; Duda, R. D.; Maheshwari, S.; Milton, R. D.; Minteer, S. D.; Janik, M. J.; Renner, J. N.; Greenlee, L. F., Catalysts for nitrogen reduction to ammonia. *Nat. Catal.* **2018,** *1* (7), 490-500, https://doi.org/10.1038/s41929-018-0092-7.
(55) Medford, A. J.; Vojvodic, A.; Hummelshøj, J. S.; Voss, J.; Abild-Pedersen, F.; Studt, F.; Bligaard, T.; Nilsson, A.; Nørskov, J. K., From the Sabatier principle to a predictive theory of transition-metal heterogeneous catalysis. *J. Catal.* **2015,** *328*, 36-42, https://doi.org/10.1016/j.jcat.2014.12.033.
(56) Wang, T.; Abild-Pedersen, F., Achieving industrial ammonia synthesis rates at near-ambient conditions through modified scaling relations on a confined dual site. *PNAS.* **2021,** *118* (30), e2106527118, https://doi.org/10.1073/pnas.2106527118.
(57) Rouwenhorst, K. H. R.; Kim, H.-H.; Lefferts, L., Vibrationally excited activation of N_2 in plasma-enhanced catalytic ammonia synthesis: A kinetic analysis. *ACS Sustain. Chem. Eng.* **2019,** *7* (20), 17515-17522, https://doi.org/10.1021/acssuschemeng.9b04997.
(58) Palma, V.; Cortese, M.; Renda, S.; Ruocco, C.; Martino, M.; Meloni, E., A review about the recent advances in selected nonthermal plasma assisted solid–gas phase chemical processes. *Nanomaterials.* **2020,** *10* (8), 1596, https://doi.org/10.3390/nano10081596.
(59) Moltved, K. A.; Kepp, K. P., The chemical bond between transition metals and oxygen: electronegativity, d-orbital effects, and oxophilicity as descriptors of metal–oxygen interactions. *J. Phys. Chem. C* **2019,** *123* (30), 18432-18444, https://doi.org/10.1021/acs.jpcc.9b04317.
(60) Hollevoet, L.; Vervloessem, E.; Gorbanev, Y.; Nikiforov, A.; De Geyter, N.; Bogaerts, A.; Martens, J. A., Energy-efficient small-scale ammonia synthesis process with plasma-enabled nitrogen oxidation and catalytic reduction of adsorbed NO_x. *ChemSusChem* **2022,** *15* (10), e202102526, https://doi.org/10.1002/cssc.202102526.
(61) Shah, J.; Wang, W.; Bogaerts, A.; Carreon, M. L., Ammonia synthesis by radio frequency plasma catalysis: Revealing the underlying mechanisms. *ACS Appl. Energy Mater.* **2018,** *1* (9), 4824-4839, https://doi.org/10.1021/acsaem.8b00898.
(62) Navascués, P.; Obrero-Pérez, J. M.; Cotrino, J.; González-Elipe, A. R.; Gómez-Ramírez, A., Unraveling discharge and surface mechanisms in plasma-assisted ammonia reactions. *ACS Sustain. Chem. Eng.* **2020,** *8* (39), 14855-14866, https://doi.org/10.1021/acssuschemeng.0c04461.
(63) Gorbanev, Y.; Vervloessem, E.; Nikiforov, A.; Bogaerts, A., Nitrogen fixation with water vapor by nonequilibrium plasma: Toward sustainable ammonia production. *ACS Sustain. Chem. Eng.* **2020,** *8* (7), 2996-3004, https://doi.org/10.1021/acssuschemeng.9b07849.
(64) Hansen, F. Y.; Henriksen, N. E.; Billing, G. D.; Guldberg, A., Catalytic synthesis of ammonia using vibrationally excited nitrogen molecules: theoretical calculation of equilibrium and rate constants. *Surf. Sci.* **1992,** *264* (1-2), 225-234, https://doi.org/10.1016/0039-6028(92)90180-E.
(65) Engelmann, Y.; van 't Veer, K.; Gorbanev, Y.; Neyts, E. C.; Schneider, W. F.; Bogaerts, A., Plasma catalysis for ammonia synthesis: A microkinetic modeling study on the contributions of Eley–Rideal reactions. *ACS Sustain. Chem. Eng.* **2021,** *9* (39), 13151-13163, https://doi.org/10.1021/acssuschemeng.1c02713.

(66) Liu, J.; Zhu, X.; Hu, X.; Zhang, F.; Tu, X., Plasma-assisted ammonia synthesis in a packed-bed dielectric barrier discharge reactor: effect of argon addition. *Vacuum.* **2022,** *197*, 110786, https://doi.org/10.1016/j.vacuum.2021.110786.

(67) Hong, J.; Pancheshnyi, S.; Tam, E.; Lowke, J. J.; Prawer, S.; Murphy, A. B., Kinetic modelling of NH_3 production in N_2–H_2 non-equilibrium atmospheric-pressure plasma catalysis. *J. Phys. D: Appl. Phys* **2017,** *50* (15), 154005, http://doi.org/10.1088/1361-6463/aaa988.

(68) Liu, T.-W.; Gorky, F.; Carreon, M. L.; Gómez-Gualdrón, D. A., Energetics of reaction pathways enabled by N and H radicals during catalytic, plasma-assisted NH_3 synthesis. *ACS Sustain. Chem. Eng.* **2022**, https://doi.org/10.1021/acssuschemeng.1c05660.

(69) Xie, D.; Sun, Y.; Zhu, T.; Fan, X.; Hong, X.; Yang, W., Ammonia synthesis and by-product formation from H_2O, H_2 and N_2 by dielectric barrier discharge combined with an Ru/Al_2O_3 catalyst. *RSC. Adv* **2016,** *6* (107), 105338-105346, https://doi.org/10.1039/C6RA21351K.

(70) Haruyama, T.; Namise, T.; Shimoshimizu, N.; Uemura, S.; Takatsuji, Y.; Hino, M.; Yamasaki, R.; Kamachi, T.; Kohno, M., Non-catalyzed one-step synthesis of ammonia from atmospheric air and water. *Green Chem.* **2016,** *18* (16), 4536-4541, https://doi.org/10.1039/C6GC01560C.

(71) Zhou, D.; Zhou, R.; Zhou, R.; Liu, B.; Zhang, T.; Xian, Y.; Cullen, P. J.; Lu, X.; Ostrikov, K., Sustainable ammonia production by non-thermal plasmas: Status, mechanisms, and opportunities. *Chem. Eng. J.* **2021,** *421*, 129544, https://doi.org/10.1016/j.cej.2021.129544.

(72) Zheng, J.; Liao, F.; Wu, S.; Jones, G.; Chen, T.-Y.; Fellowes, J.; Sudmeier, T.; McPherson, I. J.; Wilkinson, I.; Tsang, S. C. E., Efficient non-dissociative activation of dinitrogen to ammonia over lithium-promoted ruthenium nanoparticles at low pressure. *Angew. Chem. Int. Ed.* **2019,** *58* (48), 17335-17341, https://doi.org/10.1002/anie.201907171.

(73) Verheyen, C.; Silva, T.; Guerra, V.; Bogaerts, A., The effect of H_2O on the vibrational populations of CO_2 in a CO_2/H_2O microwave plasma: a kinetic modelling investigation. *Plasma Sources Sci. Technol.* **2020,** *29* (9), 095009, https://doi.org/10.1088/1361-6595/aba1c8.

(74) Gorbanev, Y.; O'Connell, D.; Chechik, V., Non-thermal plasma in contact with water: The origin of species. *Chem. Eur. J.* **2016,** *22* (10), 3496-3505, https://doi.org/10.1002/chem.201503771.

(75) Kitano, M.; Kujirai, J.; Ogasawara, K.; Matsuishi, S.; Tada, T.; Abe, H.; Niwa, Y.; Hosono, H., Low-temperature synthesis of perovskite oxynitride-hydrides as ammonia synthesis catalysts. *J. Am. Chem. Soc* **2019,** *141* (51), 20344-20353, https://doi.org/10.1021/jacs.9b10726.

(76) Foo, C.; Fellowes, J.; Fang, H.; Large, A.; Wu, S.; Held, G.; Raine, E.; Ho, P.-L.; Tang, C.; Tsang, S. C. E., Importance of hydrogen migration in catalytic ammonia synthesis over yttrium-doped barium zirconate-supported ruthenium nanoparticles: visualization of proton trap sites. *J. Phys. Chem. C* **2021,** *125* (42), 23058-23070, https://doi.org/10.1021/acs.jpcc.1c04002.

TOC Image

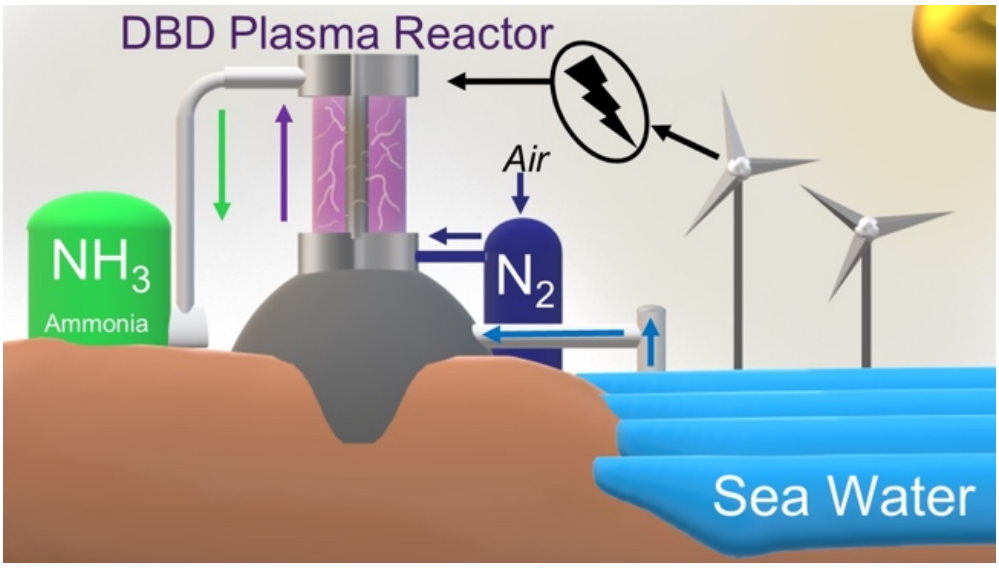

Synopsis. Non-thermal plasma driven catalytic ammonia synthesis from N_2 and seawater can be potentially used to replace for the conventional Haber–Bosch technology sustainably.